iScience

CellPress
OPEN ACCESS

Article

Network Topology Optimization of Triboelectric Nanogenerators for Effectively Harvesting Ocean Wave Energy

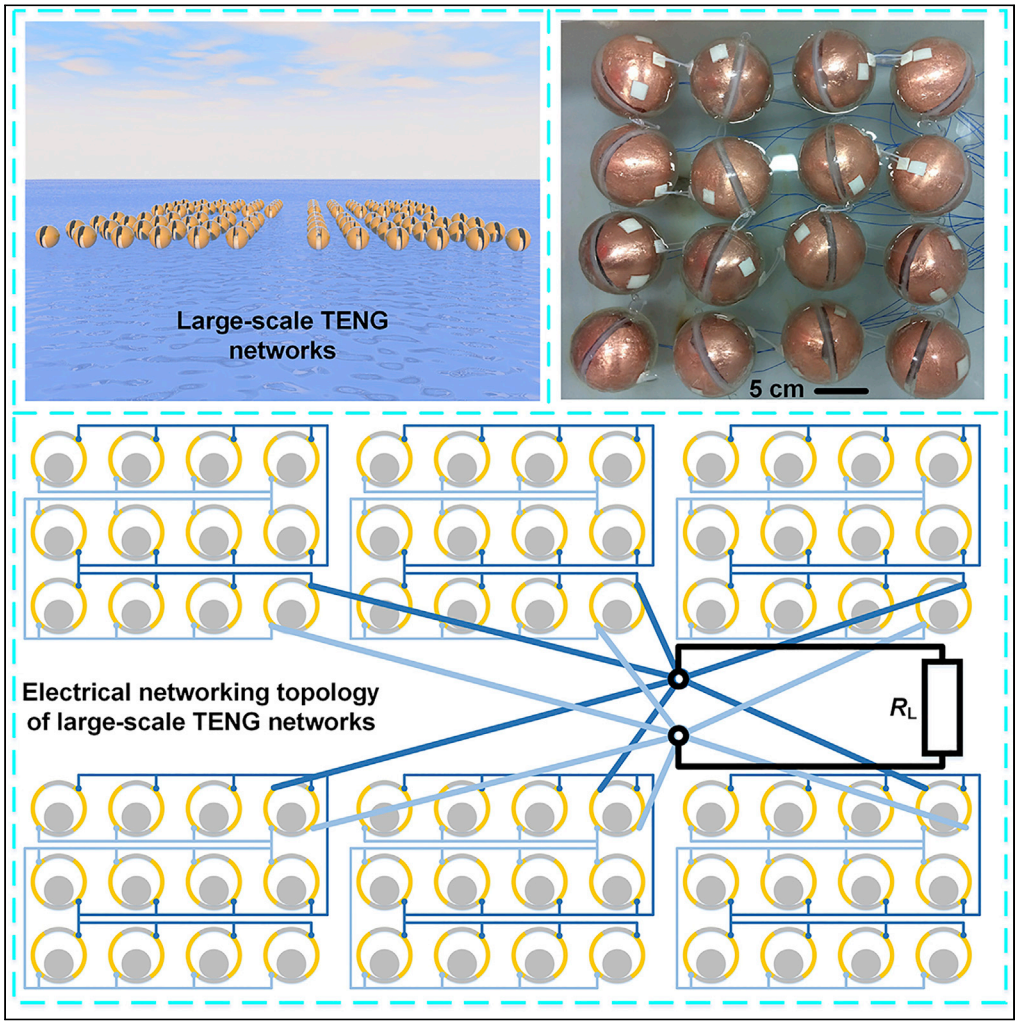

Wenbo Liu, Liang Xu, Guoxu Liu, ..., Shaohang Xu, Chunlong Fang, Chi Zhang

czhang@binn.cas.cn

HIGHLIGHTS

The effects of cable resistance and phase asynchrony to TENG networks were studied

Typical electrical networking topologies are studied that heavily impact the result

It provides a theoretical basis for optimization design of large-scale TENG networks

Liu et al., iScience *23*, 101848
December 18, 2020
https://doi.org/10.1016/j.isci.2020.101848

iScience

CellPress
OPEN ACCESS

Article

Network Topology Optimization of Triboelectric Nanogenerators for Effectively Harvesting Ocean Wave Energy

Wenbo Liu,[1,2,6] Liang Xu,[1,3,6] Guoxu Liu,[1,3] Hang Yang,[1,3] Tianzhao Bu,[1,3] Xianpeng Fu,[1,3] Shaohang Xu,[1,3] Chunlong Fang,[1,3] and Chi Zhang[1,3,4,5,*]

SUMMARY

The emerging triboelectric nanogenerator (TENG) network shows great potential in harvesting the ocean wave energy, which can help to achieve large-scale clean wave power generation. However, due to the lack of an effective networking strategy and theoretical guidance, the practicability of the TENG network is heavily restricted. In this paper, based on the typical spherical TENG, we investigated the networking design of TENGs. Four fundamental forms of electrical networking topology are proposed for large-scale TENG networks, and the influences of cable resistance and output phase asynchrony of each unit to the network output were systematically investigated. The research results show that the forms of electrical networking topology can produce an important influence on the output power of large-scale TENG networks. This is the first strategy analysis for the TENG network, which provides a theoretical basis and a universal method for the optimization design of large-scale power networks.

INTRODUCTION

With the fast development of human society, non-renewable energy such as fossil fuel is being exhausted, and the environment surrounding us is becoming worse and worse (Gielen et al., 2016; Kamat, 2007; Schiermeier et al., 2008). Humans could face an unprecedented survival crisis in the future, thus it will be urgent to develop a green and renewable energy (Brown, 1999; Chen et al, 2013, 2016, 2020a; Chen and Wang, 2017; Clery, 2008; Tollefson, 2011; Zhang et al., 2016b, 2020; Zhou et al., 2020a). Covering about 70% of Earth's surface, the ocean is magnificent and contains plenty of energy (Cho, 2015; Wang, 2017; Xi et al., 2019). The ocean wave energy has great latent capacity for development and application, while the current technology can not efficiently harvest it for various defects such as complex structure, low energy conversion efficiency, and high maintenance costs (Falcão, 2010; Scruggs and Jacob, 2009; Taylor et al., 2001; von Jouanne, 2006; Wolfbrandt, 2006). Thus, a new energy harvesting technology is needed to efficiently scavenge the energy of the ocean wave.

In 2012, Wang's group invented the triboelectric nanogenerator (TENG) based on contact electrification and electrostatic induction (Li et al, 2020a, 2020b; Wang, 2013). With the gifted advantages such as simple structure, abundant material options, and low fabrication cost (Wang, 2014; Wang et al., 2015; Zhang et al., 2014; Zhao et al., 2019), the TENGs have made remarkable achievements in the application field of micropower/nanopower sources (Ahmed et al., 2020; Chandrasekhar et al., 2017; Deng et al., 2020; Jin et al., 2020; Liu et al., 2020a; Lu et al., 2019; Quan et al., 2015; Šutka et al., 2020; Yan et al., 2020; Yang et al., 2013, 2014; Zou et al., 2020), self-powered sensors (Bu et al, 2018a, 2018b; Fu et al., 2017; Guo et al., 2018; Meng et al., 2020; Pang et al., 2015; Su et al., 2020a, 2020b; Wang et al., 2018a; Zhou et al., 2020b, 2020c), high-voltage power sources (Bu et al., 2019; Fan et al., 2015; Nie et al., 2018; Yang et al., 2019a), and large-scale blue energy (Chen et al., 2020b; Liang et al., 2019; Rodrigues et al., 2020; Xu et al, 2017, 2018; Yang et al., 2019b; Zhang et al., 2016a), which is to harvest the low frequency, irregular, and multidirectional water wave energy. Recently, some remarkable works have been developed to improve the performance of TENGs (Liu et al., 2020b, 2020c; Wang et al., 2018b). To further improve the efficiency of the TENG for harvesting water wave energy, some literatures focus on the new structures of TENGs. However, to develop large-scale water wave energy harvesting, the strategy analysis of TENG network remains to be investigated, particularly for the influence of cable resistance and output phase asynchrony of each unit.

[1]CAS Center for Excellence in Nanoscience, Beijing Key Laboratory of Micro-nano Energy and Sensor, Beijing Institute of Nanoenergy and Nanosystems, Chinese Academy of Sciences, Beijing 100083, China

[2]School of Mechanical Engineering and Automation, Beihang University, Beijing 100191, China

[3]School of Nanoscience and Technology, University of Chinese Academy of Sciences, Beijing 100049, China

[4]Center on Nanoenergy Research, School of Physical Science and Technology, Guangxi University, Nanning 530004, China

[5]Lead Contact

[6]These authors contributed equally to this work.

*Correspondence: czhang@binn.cas.cn

https://doi.org/10.1016/j.isci.2020.101848

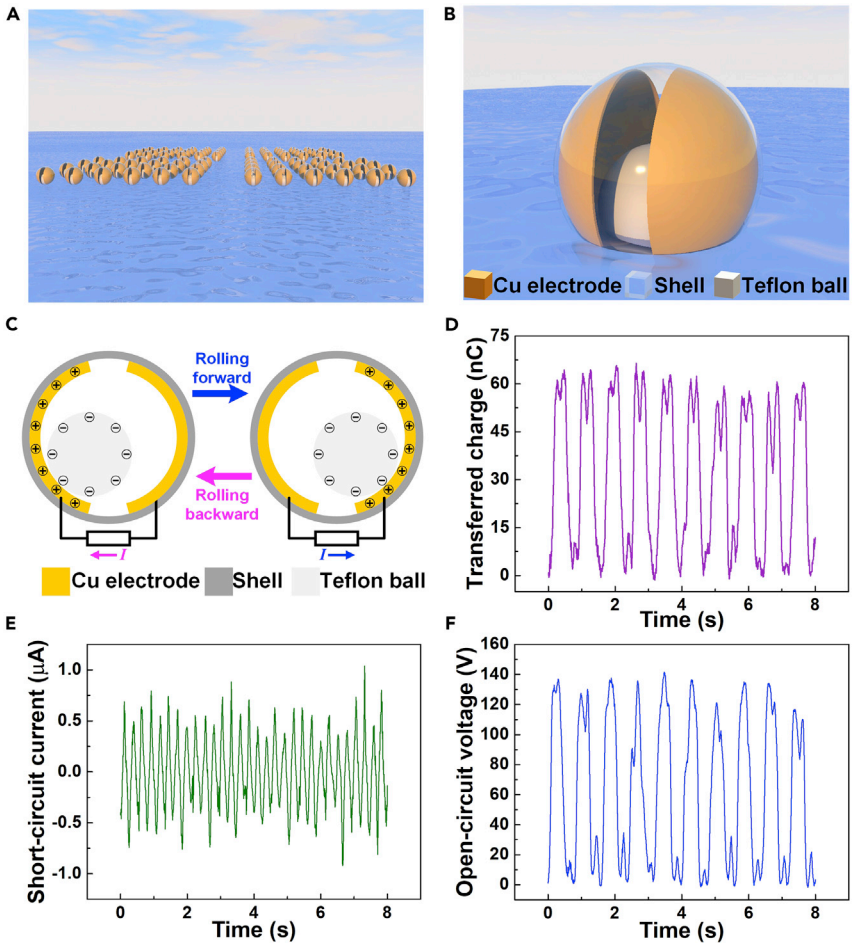

Figure 1. Structure, Working Principle, and Output Characteristics of the Spherical Triboelectric Nanogenerator

(A) Imaginary picture of future large-scale TENG network for harvesting water wave energy.

(B) Schematic structure of the spherical TENG.

(C) Working mechanism of the spherical TENG. Variation of the short-circuit transferred charges (D), the short-circuit current (E), and the shifted open-circuit voltage (F) with a water wave frequency of 1.25 Hz.

In this work, based on the typical ball-shell-structured TENG, we investigated the networking design of TENGs. Different forms of electrical networking topology are proposed for large-scale TENG networks, and the influences of cable resistance and output phase asynchrony of each unit to the network output were systematically investigated. The research results show that the network forms have an important effect on the out power of large-scale TENG networks. This is the first strategy analysis for the large-scale TENG network, which provides a theoretical basis and a universal method for optimization design of large-scale power networks.

RESULTS

Characterization of a Single TENG Unit

Figure 1A shows a schematic illustration of a large-scale TENG network on the sea for harvesting ocean blue energy. The structure of the spherical TENG is shown in Figure 1B (more details are listed in Methods). The working principle of the TENG is shown in Figure 1C. Triggered by the water wave, the Teflon ball can produce a relative motion with the shell, and the ball rolls back and forth on two copper electrodes. Based on the contact electrification, net positive charges are generated on the surface of copper which is easy to lose electrons, and net negative charges are generated on the surface of Teflon ball which has a strong ability to get electrons. During the rolling of the Teflon ball, potential difference will be built between the electrodes, driving charge transfer between them through the external circuit to maintain the equilibrium state. To simulate the

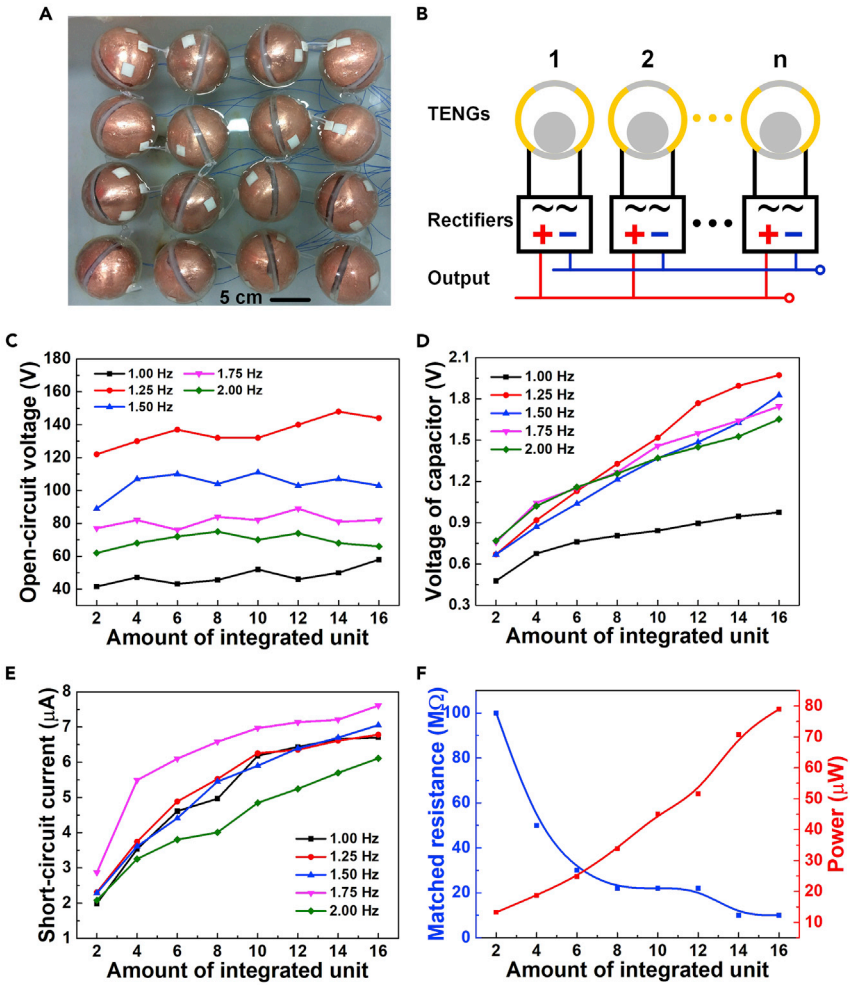

Figure 2. Output Characteristics of the Spherical TENG Network

(A) Photograph of the fabricated network.

(B) Schematic diagram of the circuit for the TENG network.

(C) The output voltage of the network when the unit amount increases from 2 to 16.

(D) The influence of unit amount on the charging performance of the TENG network.

(E) The short-circuit current of the network when the unit amount increases from 2 to 16.

(F) The effects of unit amount on the matched resistance and average power of the TENG network.

fluctuation of the sea, wave generators were fixed in a tank with water to generate water waves, as shown in Figure 1S. The frequency of water waves can be adjusted by controlling the wave generator. To present the characteristic of the spherical TENG, the short-circuit transferred charges Q_{SC}, the short-circuit current I_{SC} and the open-circuit voltage V_{OC} of the spherical TENG were experimentally tested with a water wave frequency of 1.25 Hz (The measuring instruments are list in Methods). The maximum short-circuit transferred charges Q_{SC} is 65.13 nC; the maximum short-circuit current I_{SC} is 0.66 μA, and the maximum peak-to-peak open-circuit voltage V_{OC} is 139.46 V, as shown in Figures 1D–1F, respectively. Here, the measured open-circuit voltage is shifted to above zero for demonstrating the peak-to-peak value more clearly.

Characterization of the TENG Network

To investigate the output performance of the TENG network, a 4 × 4 array is fabricated based on the spherical TENG, which is illuminated in Figure 2A. The electrical connection of the network is shown in Figure 2B, every unit in the network is rectified before being connected in parallel. Figure 2C describes the influence of the unit amount on the maximum peak-to-peak open-circuit voltage for the network with different frequencies. The voltage almost keeps invariant as the amount increases, which is due to the parallel connection of the units.

Another notable characteristic is that the output voltage of the network increases first and then decreases with the rising of the frequency. This is because that the resonance frequency of the spherical TENG is about 1.25 Hz. When the water wave frequency gets to the resonance frequency, the motion amplitude of the Teflon ball between the two electrodes is maximum. Considering that the open-circuit voltage of the device is directly related to the motion amplitude, it will also get maximized at the resonance frequency. When the water wave frequency is far away from the resonance frequency, the relative motion between the Teflon ball and the shell gets weakened, and the output also decreases. To characterize the effect of the unit amount on the transferred charges of the network, we used the TENG network to charge a capacitor of 47 μF for 30 s, and the voltage of the capacitor is shown in Figure 2D. With the increase of the unit amount, the voltage increases gradually. The maximum voltage is 1.97 V with a water wave frequency of 1.25 Hz and a unit amount of 16. As the unit amount increases, the peak of short-circuit current also improves, which is shown in Figure 2E. Moreover, the maximum short-circuit current is achieved with a wave frequency of 1.75 Hz, which is a bit higher than the resonance frequency. The reason is that the short-circuit current is the ratio between the amount of transferred charges and the charge transfer time, according to $I = dQ/dt$. When the water wave frequency increases from 1.25 Hz to 1.75 Hz, the amount of transferred charges and the charge transfer time decrease at the same time. The charge transfer time decreases larger than the amount of transferred charges, so the maximum short-circuit current is achieved with a water frequency of 1.75 Hz. As illustrated in Figure 2F, the output power of the TENG network has positive correlation with the unit amount, while the matched resistance of the network descends with the increasing of the unit amount, which is attributed to the parallel connection of the units in the TENG network.

Effect of Cable Resistance and Networking Topology

A large-scale TENG network for blue energy can include hundreds or thousands of TENGs distributed in a wide area of water, and the cables used to connect the TENGs in the network have a considerable length which should have a great impact on the output due to cable impedance. Thus, the electrical networking topology, which largely decides the cable impedance, should be optimized to minimize the negative effect. Here, four fundamental forms of networking topologies are investigated by theoretical calculations. For simplicity, we assume that all the TENGs in the network uniformly distributed in the ocean and output in the same phase. The inductance and capacitance of the cables are neglected considering the relatively low values. The period of output, open-circuit voltage, capacitance, and maximum average power of the single TENG are noted as T, V_{OC}, C, and P_0, respectively. The external load resistance of the TENG network is R_L.

The first electrical networking topology is shown in Figure 3A. According to the Fundamentals of Electric Circuits (Alexander and Sadiku, 2012), the maximum average power of the first electrical networking topology can be deduced, as shown in the following Equations 1–11. Every two adjacent TENG units are connected by cables. The length of the cable used to connect the two adjacent TENGs is l_a, and the resistance of the cable can be given as follows:

$$R_a = \frac{\rho l_a}{S} \quad \text{(Equation 1)}$$

where S and ρ are the cross-sectional area and resistivity of the cable, respectively. The schematic diagram of the lumped parameter model for the first networking topology is depicted in the left of Figure 3B, which can be simplified to the right circuit of Figure 3B based on Thévenin's theorem. Since that all the TENGs are connected in parallel, the open-circuit voltage of the entire TENG network can be described as follows:

$$V_{a,n} = V_{OC} \quad \text{(Equation 2)}$$

where n denotes the integrated number of TENG units in the network. The effective open-circuit voltage of the TENG network is given as follows:

$$U_a = \sqrt{\frac{1}{T}\int_0^T V_{a,n}^2 dt} \quad \text{(Equation 3)}$$

The relationship between the internal impedance of the TENG network $\mathbf{Z}_{a,n}$ and the amount of integrated TENG units n can be given by the following iteration equations:

$$\begin{cases} \mathbf{Z}_{a,1} = \mathbf{Z}_C \\ \mathbf{Z}_{a,n} = (\mathbf{Z}_{a,n-1} + R_a)//\mathbf{Z}_C \end{cases} \quad \text{(Equation 4)}$$

where // denotes the parallel connection operation. The internal impedance (Z_C) of each TENG in the network can be given as follows:

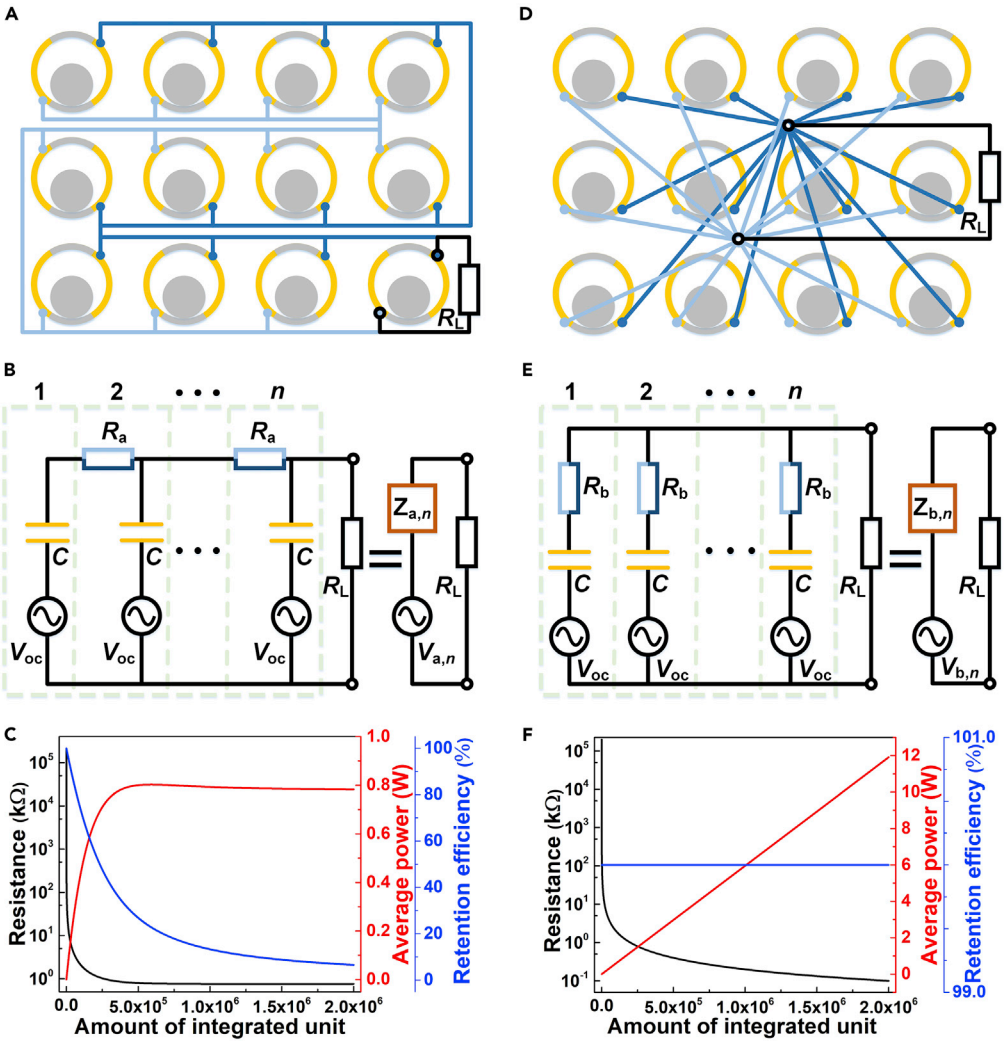

Figure 3. The First and Second Networking Topologies of the TENG Network

(A–F) Cable connection (A) and circuit model (B) for the first networking topology. (C) The dependence of the maximum average power, optimum load resistance, and retention efficiency on the amount of integrated units for the first networking topology. Cable connection (D) and circuit model (E) for the second networking topology. (F) The dependence of the maximum average power, optimum load resistance, and retention efficiency on the amount of integrated units for the second networking topology.

$$Z_C = \frac{1}{j\omega C} \quad \text{(Equation 5)}$$

The internal impedance of the TENG network can be expressed as follows:

$$Z_{a,n} = R_{a,n} + jX_{a,n} \quad \text{(Equation 6)}$$

where $R_{a,n}$ is the resistance and $X_{a,n}$ is the capacitive reactance of the TENG network.

The effective current of the TENG network can be calculated as as follows:

$$I_a = \frac{U_a}{\sqrt{(R_L + R_{a,n})^2 + X_{a,n}^2}} \quad \text{(Equation 7)}$$

Then, the average power of the TENG network can be given as follows:

$$P_a = I_a^2 R_L = \frac{U_a^2 R_L}{(R_L + R_{a,n})^2 + X_{a,n}^2} \quad \text{(Equation 8)}$$

The optimum load resistance R_{opt}, which can absorb the largest power, satisfies the following equation:

$$\frac{\partial P_a}{\partial R_L} = U_a^2 \left[\frac{\left(R_{a,n}^2 + X_{a,n}^2\right) - R_L^2}{\left[(R_L + R_{a,n})^2 + X_{a,n}^2\right]^2} \right] = 0 \quad \text{(Equation 9)}$$

Thus, the expression of R_{opt} can be given as follows:

$$R_{opt} = \sqrt{R_{a,n}^2 + X_{a,n}^2} = |Z_{a,n}| \quad \text{(Equation 10)}$$

Consecutively, the maximum average power of the network with the above condition is given as follows:

$$P_{amax} = \frac{U_a^2}{2(R_{opt} + R_{a,n})} = \frac{U_a^2}{2\left(\sqrt{R_{a,n}^2 + X_{a,n}^2} + R_{a,n}\right)} = \frac{U_a^2}{2(|Z_{a,n}| + R_{a,n})} \quad \text{(Equation 11)}$$

We define a retention efficiency as in (Equation 12), which can characterize the effect of cables and networking on the output power for the TENG network

$$\alpha_a = \frac{P_{amax}}{nP_0} \times 100\% \quad \text{(Equation 12)}$$

The dependence of R_{opt}, P_{amax}, and α_a on the amount of integrated unit n can be obtained by iterative numerical calculations. To get the results of numerical calculations, we set the initial value which can be got by experimental tests and write Python scripts according to the formula. Then, we run the scripts to get the results of numerical calculations. According to experiment results, with a water wave frequency of 1.25 Hz, the average power of a single TENG P_0 is 5.95×10^{-6} W and the capacitance C is 6.40×10^{-10} F. The cable length l_a needed to connect two adjacent units is 220 mm considering a spacing of 20 mm. The resistance of such cables is 2.20×10^{-3} Ω with a typical cross-sectional area $S = 2$ mm^2 and a typical resistivity $\rho = 2 \times 10^{-8}$ Ω•m. The calculated results are depicted in Figure 3C. For the first networking topology, the optimum load resistance R_{opt} decreases rapidly with an increasing amount of TENG units and approaches a saturated value of about 760 Ω around the quantity of 1.09×10^6. The average power shows a non-monotonic variation, achieving maximum value of 0.80 W with the amount of 5.74×10^5. The retention efficiency α_a decreases rapidly with the initial rise of the number of integrated units and then gradually saturates with the further increase of the amount.

The second electrical networking topology is shown in Figure 3D. According to the Fundamentals of Electric Circuits (Alexander and Sadiku, 2012), the maximum average power of the second electrical networking topology can be deduced, as shown in the following Equations 13–18. All the TENG units are connected at two points through cables. The length of the cable is noted as $l_{b,n}$ The schematic diagram of the lumped parameter model of the second networking topology and the simplified model is shown in Figure 3E. Supposing that all the TENGs are organized into a network of $y \times y$ array, the resistance of each cable can be expressed as follows:

$$\begin{cases} l_{b,n} = y l_a = l_a \sqrt{n} \\ R_b = \dfrac{\rho l_{b,n}}{S} \end{cases} \quad \text{(Equation 13)}$$

where n is the amount of integrated TENG units.

The relationship between the internal impedance of the TENG network $Z_{b,n}$ and the amount of integrated units n is given as follows:

$$Z_{b,n} = \frac{R_b + Z_C}{n} = \frac{R_b}{n} + \frac{1}{jn\omega C} \quad \text{(Equation 14)}$$

Since that all the TENGs are connected in parallel, the capacitive reactance of the second electrical networking topology can be expressed as follows:

$$X_{b,n} = \frac{1}{n\omega C} \quad \text{(Equation 15)}$$

The computing method of the maximum average power for this electrical networking topology is the same as that of the first electrical networking topology. Therefore, for the maximum average power of the second networking topology, the network can be expressed as follows:

$$P_{bmax} = \frac{U_b^2}{2(|Z_{b,n}| + R_{b,n})} \quad \text{(Equation 16)}$$

The retention efficiency for the second electrical networking topology can be expressed as follows:

$$\alpha_b = \frac{P_{bmax}}{nP_0} \times 100\% \quad \text{(Equation 17)}$$

The dependence of R_{opt}, P_{bmax}, and α_b on the amount of integrated units n can be obtained by numerical calculations, as depicted in Figure 3F. With the increase of unit amount, the optimum load resistance R_{opt} decays rapidly, while the maximum average power increases almost linearly. The retention efficiency α_b almost remains at 100%. Theoretical calculation results indicate that the resistance of the cable, for the second networking topology, has little effect on the output power of the TENG network. Thus, the maximum average power of the TENG network can be approximately given as follows:

$$P_b = nP_0 \quad \text{(Equation 18)}$$

The above results show that the first networking topology can lead to a significant decrease in the output power of the TENG network. However, the cables used in the first networking topology should be much less than the second topology, which are easier to be arranged and integrated with lower cost.

To take advantage of the first and the second networking topology, the third electrical networking topology is proposed with a hierarchy structure, in which the TENG network is divided into several modules (h) and each module includes multiple TENGs (m). Figure 4A shows the cable connection of the third networking topology, and the schematic diagram of the lumped parameter model and the simplified model is depicted in Figure 4B. In each module, the first networking topology is adopted for connection, and the second networking topology is used for connections among modules. The third networking topology can provide a compromising strategy between the two fundamental topologies. According to the Fundamentals of Electric Circuits (Alexander and Sadiku, 2012), the maximum average power of the thied electrical networking topology can be deduced, as shown in the following Equations 19–25.

As an example, we optimized a TENG network distributing in a water area of 1 km^2 based on the third topology. The amount of the TENGs in the network is $K = 8.26 \times 10^7$ considering a spacing of 2 cm between two adjacent TENGs. All the TENG modules are connected at two points through equal length cables l_c, which is the side length of the TENG network. The resistance of the cable used to connect each module can be given as follows:

$$\begin{cases} l_c = l_a\sqrt{n} \\ R_c = \dfrac{\rho l_c}{S} \end{cases} \quad \text{(Equation 19)}$$

and the resistance of the cable used to connect the two adjacent TENGs for each module can be expressed as follows:

$$R_{cim} = \frac{\rho l_a}{S} \quad \text{(Equation 20)}$$

The relationship between the internal impedance of the TENG network $Z_{c,h}$ and the amount of integrated modules h is given as follows:

$$Z_{c,h} = \frac{R_c + Z_m}{h} \quad \text{(Equation 21)}$$

The relationship between the internal impedance of the TENG network module Z_m and the amount of TENGs (m) in each module can be given by the following iteration equations:

$$\begin{cases} Z_1 = Z_C \\ Z_m = (Z_{m-1} + R_{cim})//Z_C \end{cases} \quad \text{(Equation 22)}$$

The internal impedance of the TENG network can be expressed as follows:

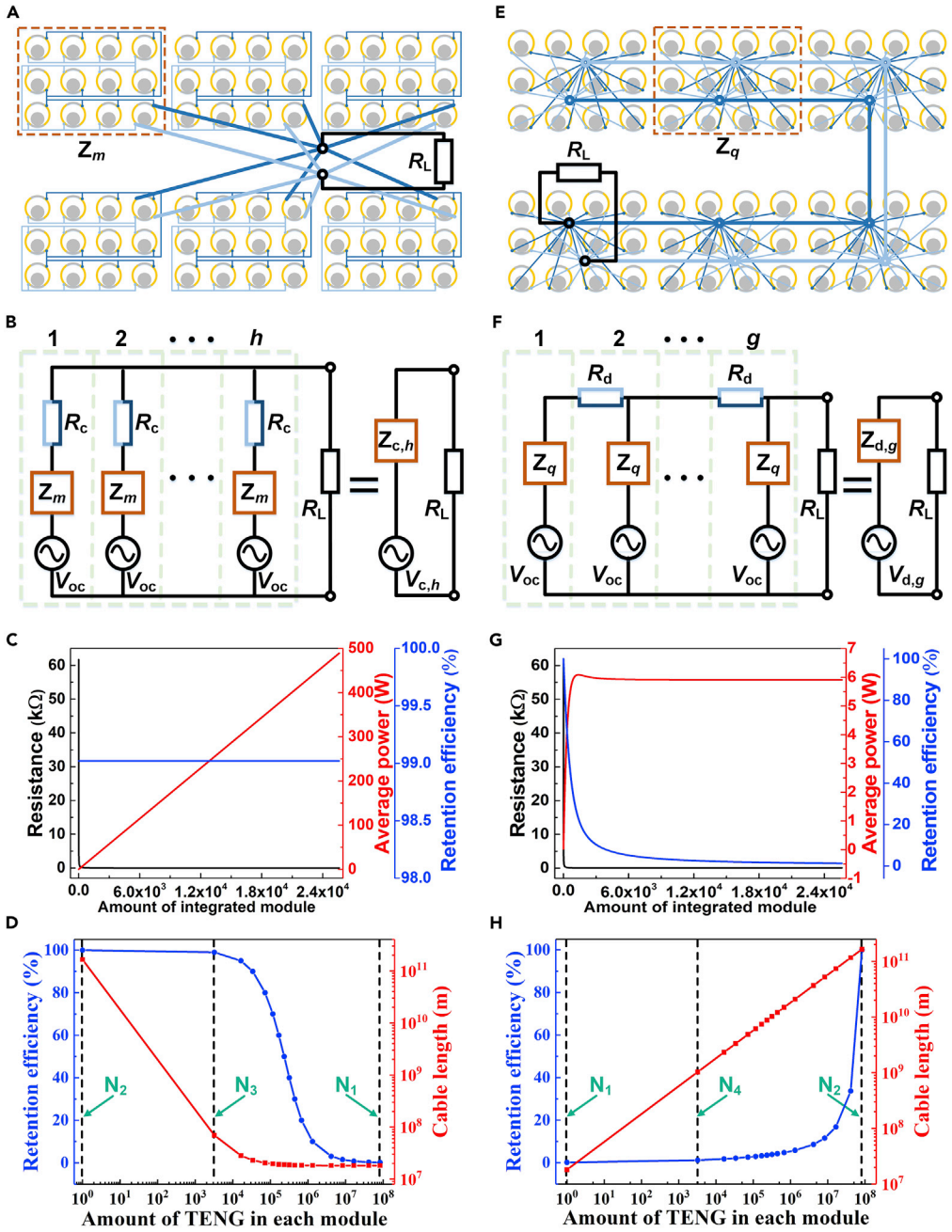

Figure 4. The Third and Fourth Networking Topologies of the TENG Network

(A and B)Cable connection (A) and circuit model (B) for the third networking topology.

(C) The dependence of the maximum average power, optimum load resistance, and retention efficiency on the amount of integrated modules for the third networking topology.

(D) The dependence of retention efficiency and cable length on the amount of TENGs in each module for the third networking topology.

(E and F) Cable connection (E) and circuit model (F) for the fourth networking topology.

(G) The dependence of the maximum average power, optimum load resistance, and retention efficiency on the amount of integrated modules for the fourth networking topology.

(H) The dependence of retention efficiency and cable length on the amount of TENGs in each module for the fourth networking topology.

$$Z_{c,h} = R_{c,h} + jX_{c,h} \quad \text{(Equation 23)}$$

where $R_{c,h}$ is the resistance and $X_{c,h}$ is the capacitive reactance of the TENG network.

The computing method of the maximum average power for this electrical networking topology is the same as that of the first electrical networking topology. Therefore, the maximum average power of the third networking topology the network can be expressed as follows:

$$P_{cmax} = \frac{U_c^2}{2(R_{opt} + R_{c,h})} = \frac{U_c^2}{2(|Z_{c,h}| + R_{c,h})} \quad \text{(Equation 24)}$$

The retention efficiency for the third networking topology is defined as follows:

$$\alpha_c = \frac{P_{cmax}}{nP_0} \times 100\% \quad \text{(Equation 25)}$$

where P_{cmax} is the maximum average power of the network for the third topology. To achieve a relatively high retention efficiency of 99%, it can be calculated using the amount of the modules (h) in the TENG network and the amount of TENG units (m) in each module. For this case, h is 2.56×10^4 and m is 3224.

With a certain amount of TENG units (3224) in each module, the dependence of R_{opt}, P_{cmax}, and α_c on the amount of integrated modules h can be obtained by numerical calculations, as depicted in Figure 4C. With the increase of module amount, the optimum load resistance R_{opt} decays rapidly, while the maximum average power increases almost linearly. The retention efficiency α_c almost remains at 99%.

Furthermore, with a certain amount of TENGs (8.26×10^7) in the TENG network, the dependence of retention efficiency and cable length on the amount of TENGs in each module for the third networking topology were calculated in Figure 4D. With the increasing of the amount of TENGs in each module, the retention efficiency shows little decline at first, then decreases rapidly. The cable length used in this whole TENG network shows fast decline. The point of N_2 represents that there is only one TENG in each module, so all the TENG units are connected at two points through cables as the second electrical networking topology. At this moment, the third electrical networking is equivalent to the second networking topology. The point of N_1 represents that all the TENGs are contained within a single module. For this case, the third electrical networking is equivalent to the first networking topology. The point of N_3 represents that there are 3224 TENG units in each module. In this case, the retention efficiency is 99% which has been calculated, while the cable length dropped by three orders of magnitude. This is significant for large TENG networks, with the decrease of the cable length, the production costs and the complexity of the TENG networks can be reduced, and the energy loss can be very low for the third networking topology.

The fourth electrical networking topology is schematically illustrated in Figure 4E, in which the TENG network is divided into several modules (g) and each module includes multiple TENGs (q). The schematic diagram of the lumped parameter model and the simplified model is depicted in Figure 4F. In each module, the second networking topology is adopted for connection, and the first networking topology is used for connections among modules. According to the Fundamentals of Electric Circuits (Alexander and Sadiku, 2012), the maximum average power of the fourth electrical networking topology can be deduced, as shown in the following Equations 26–32. The length of the cable used to connect the two adjacent modules is $l_{d,q}$, and the resistance of the cable can be given as follows:

$$\begin{cases} l_{d,q} = l_a\sqrt{q} \\ R_d = \dfrac{\rho l_{d,q}}{S} \end{cases} \quad \text{(Equation 26)}$$

All the TENG units in each module are connected at two points through equal length cable, which is the side length of the module, so the resistance of the cable used in each module can be expressed as follows:

$$R_{dim} = \frac{\rho l_a\sqrt{q}}{S} \quad \text{(Equation 27)}$$

Networking Topology	Resistance (Ω)	Power (w)	Efficiency	Cable Length (m)
First (N_1)	759.56	0.78	0.16	1.82×10^{7}
Second (N_2)	2.41	494.47	100	1.67×10^{11}
Third (N_3)	2.41	489.11	99	6.94×10^{7}
Fourth (N_4)	100.71	5.91	1.2	1.03×10^{9}

Table 1. List of Merits and Demerits for the Four Networking Topologies

The relationship between the internal impedance of the TENG network $\mathbf{Z}_{d,g}$ and the amount of integrated modules g is given as follows:

$$\begin{cases} \mathbf{Z}_{d,1} = \mathbf{Z}_q \\ \mathbf{Z}_{d,g} = \left(\mathbf{Z}_{d,g-1} + R_d\right) // \mathbf{Z}_q \end{cases} \quad \text{(Equation 28)}$$

The relationship between the internal impedance of the TENG network module $\mathbf{Z}_q$ and the amount of TENGs (q) in each module can be given by the following equation:

$$\mathbf{Z}_q = \frac{R_{dim} + \mathbf{Z}_C}{q} = \frac{R_{dim}}{q} + \frac{1}{jq\omega C} \quad \text{(Equation 29)}$$

The internal impedance of the TENG network can be expressed as follows:

$$\mathbf{Z}_{d,g} = R_{d,g} + jX_{d,g} \quad \text{(Equation 30)}$$

where $R_{d,g}$ is the resistance and $X_{d,g}$ is the capacitive reactance of the TENG network.

The computing method of the maximum average power for this electrical networking topology is the same as that of the first electrical networking topology. Therefore, for the maximum average power of the fourth networking topology, the network can be expressed as follows:

$$P_{dmax} = \frac{U_d^2}{2\left(R_{opt} + R_{d,g}\right)} = \frac{U_d^2}{2\left(\left|\mathbf{Z}_{d,g}\right| + R_{d,g}\right)} \quad \text{(Equation 31)}$$

The retention efficiency for the fourth networking topology is defined as follows:

$$\alpha_d = \frac{P_{dmax}}{nP_0} \times 100\% \quad \text{(Equation 32)}$$

For the sake of comparison and evaluation, with the same amount of TENG units (3224) in each module as the third networking topology, the dependence of R_{opt}, P_{dmax}, and α_d on the amount of integrated modules g can be obtained by numerical calculations, as depicted in Figure 4G. The optimum load resistance R_{opt} decreases rapidly with an increasing amount of TENG units and approaches a saturated value of about 100.71 Ω. The average power shows a non-monotonic variation, achieving a maximum value of 6.09 W with the module amount of 1397. The retention efficiency α_d decreases rapidly with the initial rise of the number of integrated modules and then gradually saturates with the further increase of the amount and reaches to 1.2% at last.

What's more, with a certain amount of TENGs (8.26×10^7) in the TENG network, the dependence of retention efficiency and cable length on the amount of TENGs in each module for the fourth networking topology were calculated in Figure 4H. With the increasing of the amount of TENGs in each module, the retention efficiency increases rapidly, and the cable length used in this whole TENG network rises. With the increase of the cable length, the production costs and the complexity of the TENG networks can grow, while the retention efficiency of the network would also be improved. The point of N_1 represents that there is only one TENG in each module, so all the TENG units are connected as the first electrical networking topology. At this moment, the fourth electrical networking is equivalent to the first networking topology. The point of N_2 represents that all the TENGs are contained within a single module. For this case, the fourth electrical networking is equivalent to the second networking topology. The point of N_4 represents that there are 3224 TENG units in each module. In this case, the retention efficiency for this case is 1.2% which is much lower than that of the third networking topology.

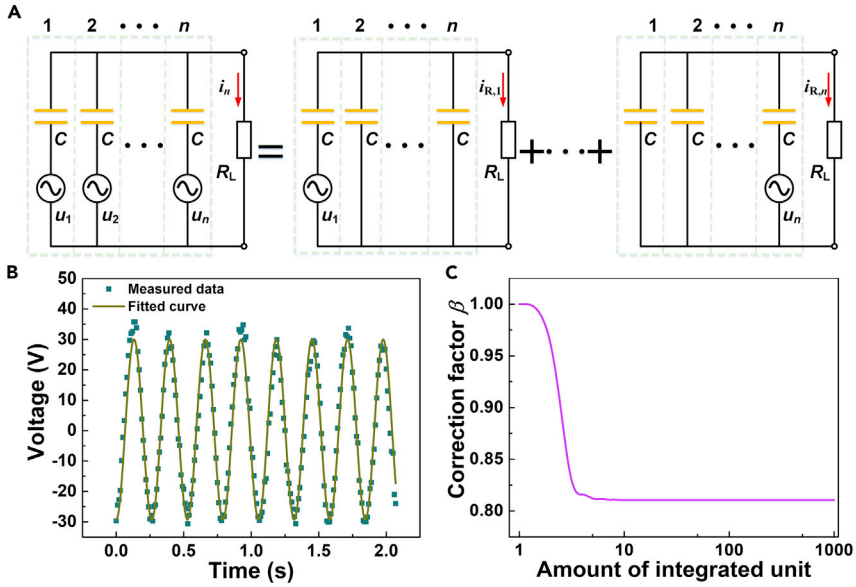

Figure 5. Influence of the Output Phase Asynchrony

(A) Schematic diagram of the circuit model for the TENG network.

(B) The fitting curve for the output voltage of the spherical TENG.

(C) Dependence of the correction factor β on the amount of integrated units.

To clearly show the merits and demerits of these four networking topologies, the optimum load resistance, the maximum average power, the retention efficiency, and the cable length used in TENG networks are summarized in Table 1 for above calculated cases with the same TENG unit and network scale. With the third networking topology, the TENG network can maintain high efficiency with relatively less amount of cables. For example, at the point of N_3, the retention efficiency of the TENG network only decreases 1%, while the cable length used in the TENG network dropped by three orders of magnitude. That is meaningful to large-scale TENG networks because the decrease of cable length can not only reduce the production costs of the TENG networks but also lower the complexity of the TENG networks. Therefore, the third networking topology can facilitate the practical application of TENG networks in large-scale water wave energy, further implementing the blue energy dream.

The above topology optimization methods can be applied in TENG networks of any scale to improve the performance. The reason is that the scale of TENG networks will not affect the optimization process of electrical networking topology. It can be optimized, once the amounts of the units in TENG networks are determined. For TENG networks with multiple layers, the efficiency can be calculated similarly.

The network topology optimization method can also be applied to other structures of TENGs, as a universal method. The reason why we use the spherical TENG here is that it is a typical structure in water wave energy harvesting, which can make the theoretical work more easily understood. The structures of TENGs can only influence the initial values of numerical optimization calculation such as the period of output, open-circuit voltage, and capacitance of the single TENG, while those values of TENG output do not affect the major optimization process of the networking.

Effect of Output Phase Asynchrony

The TENG has an alternative output; thus, the output phase asynchrony for all the TENG units in the network should greatly influence the total output of the network, which is theoretically analyzed here. We consider a simplified situation where the cable resistance is neglected, and the lumped parameter model of the TENG network is illustrated in the left of Figure 5A, with a purely resistive load. The model should be a linear system with independent sources and linear components, so the superposition theorem

can be applied and the model is equivalent to the superposition of a series of models demonstrated in the right of Figure 5A. According to the Fundamentals of Electric Circuits (Alexander and Sadiku, 2012), the influence of output phase asynchrony for all the TENG units can be deduced, as shown in the following Equations 34–41. The stable current output of the TENG network through the load resistor can be expressed as follws:

$$i_n = i_{R,1} + i_{R,2} + \cdots + i_{R,n} \quad \text{(Equation 33)}$$

where $i_{R,n}$ is the current in the nth model for superposition. The experimental measured output voltage of a single TENG can be fitted well by a sinusoidal curve, as shown in Figure 5B. Therefore, similarly, we describe the voltage on a load using the following expression:

$$u_k = U\sin(\omega t + \phi_{u,k}) \quad \text{(Equation 34)}$$

where U is the amplitude of the output voltage, ω is the angular frequency, and $\phi_{u,k}$ is the initial phase angle of the kth TENG unit. The amplitude U and the angular frequency ω are assumed to be the same for all the TENG units for simplification. For the linear circuit shown in Figure 5A, such voltage corresponds to a current of sinusoidal form with the same angular frequency. Therefore, the current can be described as follows:

$$i_{R,k} = I\sin(\omega t + \phi_{i,k}) \quad \text{(Equation 35)}$$

where I is the amplitude of the current and $\phi_{i,k}$ is the initial phase angle of the current. When the output of all the TENG units in the TENG network is completely synchronous with the same phase, the average output power can be calculated as follows:

$$P_e = \frac{\int_0^T i_n^2 R_L dt}{T} = \frac{R_L n^2 I^2 \int_0^T [\sin(\omega t + \phi_{i,n})]^2 dt}{T} = \frac{n^2 I^2 R_L}{2} \quad \text{(Equation 36)}$$

where T is the period of the output current for each unit. Considering the practical application of the TENG network in water, the TENG units can hardly output in a synchronized way. While the amount of the TENGs increases, the phase angles tend to uniformly distribute within (0, 2π) with asynchrony. In such a case, rectifiers are often used in the circuit for each unit. According to (Equation 33), the current of the TENG network through the resistor R_L can be described as follows:

$$i_n = I\left|\sin\left(\omega t + \frac{2\pi}{n}\right)\right| + I\left|\sin\left(\omega t + \frac{4\pi}{n}\right)\right| + I\left|\sin\left(\omega t + \frac{6\pi}{n}\right)\right| + \cdots + I|\sin(\omega t + 2\pi)|$$

$$= I\sum_{k=1}^{n}\left|\sin\left(\omega t + \frac{2k\pi}{n}\right)\right| \quad \text{(Equation 37)}$$

In a single period of T, the absorbed energy by the load resistor can be calculated as follows:

$$E = \int_0^T i_n^2 R_L dt = R_L I^2 \int_0^T \left[\sum_{k=1}^{n}\left|\sin\left(\omega t + \frac{2k\pi}{n}\right)\right|\right]^2 dt \quad \text{(Equation 38)}$$

Therefore, the average power of the TENG network can be expressed as follows:

$$P_f = \frac{E}{T} = \frac{R_L I^2 \int_0^T \left[\sum_{k=1}^{n}\left|\sin\left(\omega t + \frac{2k\pi}{n}\right)\right|\right]^2 dt}{T} \quad \text{(Equation 39)}$$

In order to clearly characterize the effect of the output phase asynchrony in the TENG network, a correction factor β is defined as follows:

$$\beta = \frac{P_f}{P_e} = \frac{2\int_0^T \left[\sum_{k=1}^{n}\left|\sin\left(\omega t + \frac{2k\pi}{n}\right)\right|\right]^2 dt}{Tn^2} \quad \text{(Equation 40)}$$

The parameter β is the ratio between the average output power of TENG networks with phase asynchrony and the average output power of TENG networks without phase asynchrony. The dependence of the correction factor β on the amount of TENG units n can be obtained by numerical calculations, as shown in Figure 5C. The correction factor β decreases rapidly with an initial increase of the quantity of integrated TENGs, then saturates at about 0.81 with the further increase of the amount.

Considering the cable resistance and the output phase asynchrony, the maximum average power of the TENG network with the third networking topology and matched resistance can be expressed as follows:

$$P = n\alpha_c\beta P_0 \quad \text{(Equation 41)}$$

According to the above theoretical analyses, with a water wave frequency of 1.25 Hz, the maximum average power is expected to be 14.22 kW from a TENG network that covers 1 km^2 water area with a depth of 5 m. The amounts of the TENG network layers are 45 with setting the spacing between every two adjacent layers as 2 cm.

DISCUSSION

In summary, we have fabricated TENG networks based on spherical TENG units and then demonstrated the effects of water wave frequency and the amount of TENG units on the performance of the TENG network. Moreover, four fundamental forms of electrical networking topology have been proposed for large-scale TENG networks, and the influences of cable resistance and output phase asynchrony of each unit to the network output were systematically investigated. The research results show that the network forms can produce an important influence on the output power of large-scale TENG networks. This is the first strategy analysis for the TENG network, which provides a theoretical basis and a universal method for optimization design of large-scale power networks.

Limitations of the Study

Four fundamental forms of electrical networking topology were proposed for large-scale TENG networks, and the influences of cable resistance and output phase asynchrony of each unit to the network output were systematically investigated, which have provided a theoretical basis and a universal method for the optimization design of large-scale power networks. However, experimental investigation can be conducted to further validate, refine, and extend the theoretical calculation models for the four fundamental forms of electrical networking topology.

Resource Availability

Lead Contact

Further information and requests for resources and reagents should be directed to and will be fulfilled by the Lead Contact, Chi Zhang (czhang@binn.cas.cn).

Materials Availability

This study did not generate new unique reagents.

Data and Code Availability

We do not have any code and upon request we can provide the original data.

METHODS

All methods can be found in the accompanying Transparent Methods supplemental file.

SUPPLEMENTAL INFORMATION

Supplemental Information can be found online at https://doi.org/10.1016/j.isci.2020.101848.

ACKNOWLEDGMENTS

The authors thank the support of the National Key Research and Development Program of China (2016YFA0202704), National Natural Science Foundation of China (Nos. 51922023, 61874011), and Beijing Natural Science Foundation (No. 4192070).

AUTHOR CONTRIBUTIONS

W.L., L.X., and C.Z. designed the experiments, analyzed the data, and wrote the paper. W.L., G.L., and H.Y. carried out the experiments, discussed the results, and performed theoretical calculations. T.B., X.F., S.X., and C.F. discussed the results and assisted with experiments.

DECLARATION OF INTERESTS

All authors confirm there are no competing interests.

Received: September 30, 2020
Revised: November 7, 2020
Accepted: November 18, 2020
Published: December 18, 2020

REFERENCES

Ahmed, A., Hassan, I., Helal, A.S., Sencadas, V., Radhi, A., Jeong, C.K., and El-Kady, M.F. (2020). Triboelectric nanogenerator versus piezoelectric generator at low frequency (<4 Hz): a quantitative comparison. iScience *23*, 101286.

Alexander, Charles, K., Sadiku, and Matthew, N.O. (2012). Fundamentals of Electric Circuits (McGraw Hill Higher Education).

Brown, K.S. (1999). Bright future–or brief flare–for renewable energy? Science *285*, 678–680.

Bu, T., Jiang, D., Yang, X., Liu, W., Liu, G., Guo, T., Pang, Y., Zhao, J., Xi, F., and Zhang, C. (2018a). Liquid metal gated tribotronic transistors as an electronic gradienter for angle measurement. Adv. Electron. Mater. *4*, 1800269.

Bu, T., Xiao, T., Yang, Z., Liu, G., Fu, X., Nie, J., Guo, T., Pang, Y., Zhao, J., Xi, F., et al. (2018b). Stretchable triboelectric-photonic smart skin for tactile and gesture sensing. Adv. Mater. *30*, 1800066.

Bu, T., Yang, H., Liu, W., Pang, Y., Zhang, C., and Wang, Z.L. (2019). Triboelectric effect-driven liquid metal actuators. Soft Robot *6*, 664–670.

Chen, G., Li, Y., Bick, M., and Chen, J. (2020a). Smart textiles for electricity generation. Chem. Rev. *120*, 3668–3720.

Chen, H., Xing, C., Li, Y., Wang, J., and Xu, Y. (2020b). Triboelectric nanogenerators for a macro-scale blue energy harvesting and self-powered marine environmental monitoring system. Sustain. Energy Fuels *4*, 1063–1077.

Chandrasekhar, A., Alluri, N.R., Vivekananthan, V., Purusothaman, Y., and Kim, S.J. (2017). A sustainable freestanding biomechanical energy harvesting smart backpack as a portable-wearable power source. J. Mater. Chem. C *5*, 1488–1493.

Chen, J., Huang, Y., Zhang, N., Zou, H., Liu, R., Tao, C., Fan, X., and Wang, Z.L. (2016). Micro-cable structured textile for simultaneously harvesting solar and mechanical energy. Nat. Energy *1*, 16138.

Chen, J., and Wang, Z.L. (2017). Reviving vibration energy harvesting and self-powered sensing by a triboelectric nanogenerator. Joule *1*, 480–521.

Chen, J., Zhu, G., Yang, W., Jing, Q., Bai, P., Yang, Y., Hou, T.-C., and Wang, Z.L. (2013). Harmonic-resonator-based triboelectric nanogenerator as a sustainable power source and a self-powered active vibration sensor. Adv. Mater. *25*, 6094–6099.

Cho, A. (2015). To catch a wave. Science *347*, 1084–1088.

Clery, D. (2008). U.K. ponders world's biggest tidal power scheme. Science *320*, 1574.

Deng, W., Zhou, Y., Zhao, X., Zhang, S., Zou, Y., Xu, J., Yeh, M.-H., Guo, H., and Chen, J. (2020). Ternary electrification layered architecture for high-performance triboelectric nanogenerators. ACS Nano *14*, 9050–9058.

Falcão, A.F.D.O. (2010). Wave energy utilization: a review of the technologies. Renew. Sustain. Energy Rev. *14*, 899–918.

Fan, X., Chen, J., Yang, J., Bai, P., Li, Z., and Wang, Z.L. (2015). Ultrathin, rollable, paper-based triboelectric nanogenerator for acoustic energy harvesting and self-powered sound recording. ACS Nano *9*, 4236–4243.

Fu, X.P., Bu, T.Z., Xi, F. Ben, Cheng, T.H., Zhang, C., and Wang, Z.L. (2017). Embedded triboelectric active sensors for real-time pneumatic monitoring. ACS Appl. Mater. Interfaces *9*, 32352–32358.

Gielen, D., Boshell, F., and Saygin, D. (2016). Climate and energy challenges for materials science. Nat. Mater. *15*, 117–120.

Guo, T., Zhao, J., Liu, W., Liu, G., Pang, Y., Bu, T., Xi, F., Zhang, C., and Li, X. (2018). Self-powered hall vehicle sensors based on triboelectric nanogenerators. Adv. Mater. Technol. *3*, 1800140.

Jin, L., Xiao, X., Deng, W., Nashalian, A., He, D., Raveendran, V., Yan, C., Su, H., Chu, X., Yang, T., et al. (2020). Manipulating relative permittivity for high-performance wearable triboelectric nanogenerators. Nano Lett. *20*, 6404–6411.

Kamat, P.V. (2007). Meeting the clean energy demand: nanostructure architectures for solar energy conversion. J. Phys. Chem. C *111*, 2834–2860.

Li, S., Fan, Y., Chen, H., Nie, J., Liang, Y., Tao, X., Zhang, J., Chen, X., Fu, E., and Wang, Z.L. (2020a). Manipulating the triboelectric surface charge density of polymers by low-energy helium ion irradiation/implantation. Energy Environ. Sci. *13*, 896–907.

Li, S., Nie, J., Shi, Y., Tao, X., Wang, F., Tian, J., Lin, S., Chen, X., and Wang, Z.L. (2020b). Contributions of different functional groups to contact electrification of polymers. Adv. Mater. *32*, 2001307.

Liang, X., Jiang, T., Liu, G., Xiao, T., Xu, L., Li, W., Xi, F., Zhang, C., and Wang, Z.L. (2019). Triboelectric nanogenerator networks integrated with power management module for water wave energy harvesting. Adv. Funct. Mater. *29*, 1807241.

Liu, G., Xu, S., Liu, Y., Gao, Y., Tong, T., Qi, Y., and Zhang, C. (2020a). Flexible drug release device powered by triboelectric nanogenerator. Adv. Funct. Mater. *30*, 1909886.

Liu, W., Wang, Z., Wang, G., Zeng, Q., He, W., Liu, L., Wang, X., Xi, Y., Guo, H., Hu, C., and Wang, Z.L. (2020b). Switched-capacitor-convertors based on fractal design for output power management of triboelectric nanogenerator. Nat. Commun. *11*, 1–10.

Liu, Y., Liu, W., Wang, Z., He, W., Tang, Q., Xi, Y., Wang, X., Guo, H., and Hu, C. (2020c). Quantifying contact status and the air-breakdown model of charge-excitation triboelectric nanogenerators to maximize charge density. Nat. Commun. *11*, 1–8.

Lu, Y., Hao, Z., Feng, S., Shen, R., Yan, Y., and Lin, S. (2019). Direct-current generator based on dynamic PN junctions with the designed voltage output. iScience *22*, 58–69.

Meng, K., Zhao, S., Zhou, Y., Wu, Y., Zhang, S., He, Q., Wang, X., Zhou, Z., Fan, W., Tan, X., et al. (2020). A wireless textile-based sensor system for self-powered personalized health care. Matter *2*, 896–907.

Nie, J., Ren, Z., Shao, J., Deng, C., Xu, L., Chen, X., Li, M., and Wang, Z.L. (2018). Self-powered microfluidic transport system based on triboelectric nanogenerator and electrowetting technique. ACS Nano *12*, 1491–1499.

Pang, Y.K., Li, X.H., Chen, M.X., Han, C.B., Zhang, C., and Wang, Z.L. (2015). Triboelectric nanogenerators as a self-powered 3D acceleration sensor. ACS Appl. Mater. Interfaces *7*, 19076–19082.

Quan, T., Wang, X., Wang, Z.L., and Yang, Y. (2015). Hybridized electromagnetic–triboelectric nanogenerator for a self-powered electronic watch. ACS Nano *9*, 12301–12310.

Rodrigues, C., Nunes, D., Clemente, D., Mathias, N., Correia, J.M., Rosa-Santos, P., Taveira-Pinto, F., Morais, T., Pereira, A., and Ventura, J. (2020). Emerging triboelectric nanogenerators for ocean wave energy harvesting: state of the art and future perspectives. Energy Environ. Sci. *13*, 2657–2683.

Schiermeier, Q., Tollefson, J., Scully, T., Witze, A., and Morton, O. (2008). Energy alternatives: electricity without carbon. Nature *454*, 816–823.

Scruggs, J., and Jacob, P. (2009). Harvesting ocean wave energy. Science *323*, 1176–1178.

Su, Y., Wang, J., Wang, B., Yang, T., Yang, B., Xie, G., Zhou, Y., Zhang, S., Tai, H., Cai, Z., et al. (2020a). Alveolus-inspired active membrane

sensors for self-powered wearable chemical sensing and breath analysis. ACS Nano *14*, 6067–6075.

Su, Y., Yang, T., Zhao, X., Cai, Z., Chen, G., Yao, M., Chen, K., Bick, M., Wang, J., Li, S., et al. (2020b). A wireless energy transmission enabled wearable active acetone biosensor for non-invasive prediabetes diagnosis. Nano Energy *74*, 104941.

Šutka, A., Mālnieks, K., Lapčinskis, L., Timusk, M., Pudzs, K., and Rutkis, M. (2020). Matching the directions of electric fields from triboelectric and ferroelectric charges in nanogenerator devices for boosted performance. iScience *23*, 101011.

Taylor, G.W., Burns, J.R., Kammann, S.A., Powers, W.B., and Welsh, T.R. (2001). The energy harvesting eel: a small subsurface ocean/river power generator. IEEE J. Ocean. Eng. *26*, 539–547.

Tollefson, J. (2011). How green is my future? Nature *473*, 134–135.

von Jouanne, A. (2006). Harvesting the waves. Mech. Eng. *128*, 24–27.

Wang, Z., Ruan, Z., Ng, W.S., Li, H., Tang, Z., Liu, Z., Wang, Y., Hu, H., and Zhi, C. (2018b). Integrating a triboelectric nanogenerator and a zinc-ion battery on a designed flexible 3D spacer fabric. Small Methods *2*, 1800150.

Wang, Z.L. (2017). Catch wave power in floating nets. Nature *542*, 159–160.

Wang, Z.L. (2014). Triboelectric nanogenerators as new energy technology and self-powered sensors - Principles, problems and perspectives. Faraday Discuss *176*, 447–458.

Wang, Z.L. (2013). Triboelectric nanogenerators as new energy technology for self-powered systems and as active mechanical and chemical sensors. ACS Nano *7*, 9533–9557.

Wang, Z.L., Chen, J., and Lin, L. (2015). Progress in triboelectric nanogenerators as a new energy technology and self-powered sensors. Energy Environ. Sci. *8*, 2250–2282.

Wang, J., Wu, B., Liu, G., Bu, T., Guo, T., Pang, Y., Fu, X., Zhao, J., Xi, F., and Zhang, C. (2018a). Flexure hinges based triboelectric nanogenerator by 3D printing. Extrem. Mech. Lett. *20*, 38–45.

Wolfbrandt, A. (2006). Automated design of a linear generator for wave energy converters-a simplified model. IEEE Trans. Magn. *42*, 1812–1819.

Xi, F., Pang, Y., Liu, G., Wang, S., Li, W., Zhang, C., and Wang, Z.L. (2019). Self-powered intelligent buoy system by water wave energy for sustainable and autonomous wireless sensing and data transmission. Nano Energy *61*, 1–9.

Xu, L., Jiang, T., Lin, P., Shao, J.J., He, C., Zhong, W., Chen, X.Y., and Wang, Z.L. (2018). Coupled triboelectric nanogenerator networks for efficient water wave energy harvesting. ACS Nano *12*, 1849–1858.

Xu, L., Pang, Y., Zhang, C., Jiang, T., Chen, X., Luo, J., Tang, W., Cao, X., and Wang, Z.L. (2017). Integrated triboelectric nanogenerator array based on air-driven membrane structures for water wave energy harvesting. Nano Energy *31*, 351–358.

Yan, C., Gao, Y., Zhao, S., Zhang, S., Zhou, Y., Deng, W., Li, Z., Jiang, G., Jin, L., Tian, G., et al. (2020). A linear-to-rotary hybrid nanogenerator for high-performance wearable biomechanical energy harvesting. Nano Energy *67*, 104235.

Yang, H., Pang, Y., Bu, T., Liu, W., Luo, J., Jiang, D., Zhang, C., and Wang, Z.L. (2019a). Triboelectric micromotors actuated by ultralow frequency mechanical stimuli. Nat. Commun. *10*, 2309.

Yang, X., Xu, L., Lin, P., Zhong, W., Bai, Y., Luo, J., Chen, J., and Wang, Z.L. (2019b). Macroscopic self-assembly network of encapsulated high-performance triboelectric nanogenerators for water wave energy harvesting. Nano Energy *60*, 404–412.

Yang, J., Chen, J., Liu, Y., Yang, W., Su, Y., and Wang, Z.L. (2014). Triboelectrification-based organic film nanogenerator for acoustic energy harvesting and self-powered active acoustic sensing. ACS Nano *8*, 2649–2657.

Yang, W., Chen, J., Zhu, G., Yang, J., Bai, P., Su, Y., Jing, Q., Cao, X., and Wang, Z.L. (2013). Harvesting energy from the natural vibration of human walking. ACS Nano *7*, 11317–11324.

Zhang, C., Tang, W., Han, C., Fan, F., and Wang, Z.L. (2014). Theoretical comparison, equivalent transformation, and conjunction operations of electromagnetic induction generator and triboelectric nanogenerator for harvesting mechanical energy. Adv. Mater. *26*, 3580–3591.

Zhang, L.M., Han, C.B., Jiang, T., Zhou, T., Li, X.H., Zhang, C., and Wang, Z.L. (2016a). Multilayer wavy-structured robust triboelectric nanogenerator for harvesting water wave energy. Nano Energy *22*, 87–94.

Zhang, N., Chen, J., Huang, Y., Guo, W., Yang, J., Du, J., Fan, X., and Tao, C. (2016b). A wearable all-solid photovoltaic textile. Adv. Mater. *28*, 263–269.

Zhang, N., Huang, F., Zhao, S., Lv, X., Zhou, Y., Xiang, S., Xu, S., Li, Y., Chen, G., Tao, C., et al. (2020). Photo-rechargeable fabrics as sustainable and robust power sources for wearable bioelectronics. Matter *2*, 1260–1269.

Zhao, J., Zhen, G., Liu, G., Bu, T., Liu, W., Fu, X., Zhang, P., Zhang, C., and Wang, Z.L. (2019). Remarkable merits of triboelectric nanogenerator than electromagnetic generator for harvesting small-amplitude mechanical energy. Nano Energy *61*, 111–118.

Zhou, Y., Deng, W., Xu, J., and Chen, J. (2020a). Engineering materials at the nanoscale for triboelectric nanogenerators. Cell Rep. Phys. Sci. *1*, 100142.

Zhou, Z., Chen, K., Li, X., Zhang, S., Wu, Y., Zhou, Y., Meng, K., Sun, C., He, Q., Fan, W., et al. (2020b). Sign-to-speech translation using machine-learning-assisted stretchable sensor arrays. Nat. Electron. *3*, 571–578.

Zhou, Z., Padgett, S., Cai, Z., Conta, G., Wu, Y., He, Q., Zhang, S., Sun, C., Liu, J., Fan, E., et al. (2020c). Single-layered ultra-soft washable smart textiles for all-around ballistocardiograph, respiration, and posture monitoring during sleep. Biosens. Bioelectron. *155*, 112064.

Zou, Y., Raveendran, V., and Chen, J. (2020). Wearable triboelectric nanogenerators for biomechanical energy harvesting. Nano Energy *77*, 105303.

iScience, Volume *23*

Supplemental Information

Network Topology Optimization of Triboelectric Nanogenerators for Effectively Harvesting Ocean Wave Energy

Wenbo Liu, Liang Xu, Guoxu Liu, Hang Yang, Tianzhao Bu, Xianpeng Fu, Shaohang Xu, Chunlong Fang, and Chi Zhang

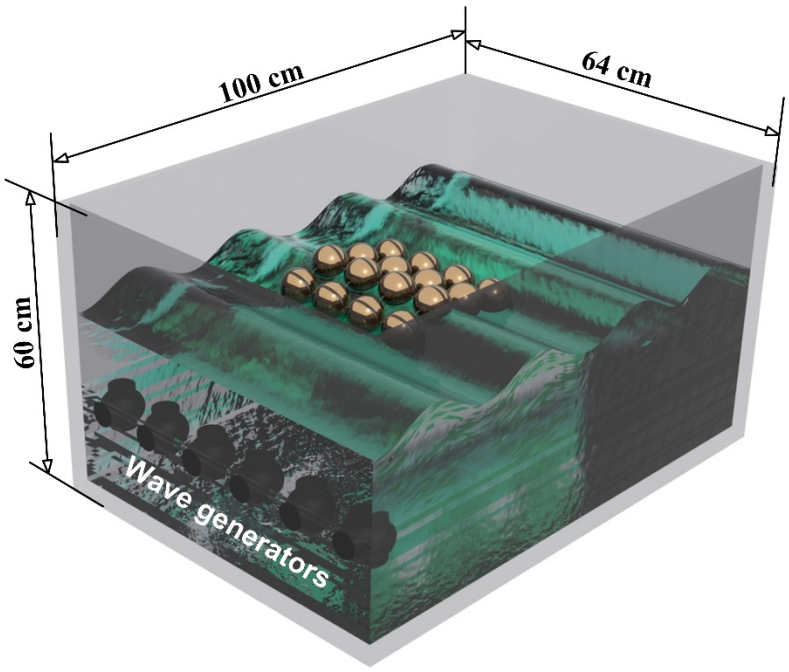

Figure 1S, related to Figure 2. Setup for experimental test

Transparent Methods

Experimental Section

Fabrication of the TENG Unit.

The spherical TENG is composed of a shell, a Teflon ball and two copper electrodes, as depicted in Figure 1b. In the fabrication of the device, firstly, two copper electrodes were attached to the inner face of two polystyrenes (PS) hemisphere (with a radius of 4 cm), respectively. Secondly, a Teflon ball was put into one of the hemispheres, then the two hemispheres were stuck together with an adhesive, forming a spherical shell. Finally, the spherical shell is wrapped by another spherical shell (with a radius of 4.5 cm) to ensure waterproof performance.

Fabrication of the Network. There exist 16 spherical TENG units, integrated them

with 4×4 arrays. Every two neighboring TENG units in the network are mechanically connected by nylon cable ties. The gap in every two neighboring TENG units is 2 cm.

Electrical Characterization.

The voltage, the transferred charges and the currents were measured by an electrometer (Keithley 6514). The voltage used to calculate output power was measured by an oscilloscope (Tektronix, MDO 3014) with a 100 MΩ probe.